3-24-2016

Hydrogen Effects on X80 Steel Mechanical Properties Measured by Tensile and Impact Testing

Xuan Li

Hydrogen Effects on X80 Steel Mechanical Properties Measured by Tensile and Impact Testing

by

Xuan Li

A thesis submitted in partial fulfillment
of the requirements for the degree of
Master of Science in Mechanical Engineering
Department of Mechanical Engineering
College of Engineering
University of South Florida

Major Professor: Alex A. Volinsky, Ph.D.
Wenjun Cai, Ph.D.
Rasim Guldiken, Ph.D.

Date of Approval:
March 11, 2016

Keywords: Hydrogen permeation, Cathodic charging, Hydrogen embrittlement, Slow strain rate tensile (SSRT) test, Charpy impact test

DEDICATION

To my beloved parents, Keqing Li and Shijuan Ma, who have been sources of encouragement and inspiration to me throughout my life. A very special thank you for driving me to the lab in the early morning and picking me up at late midnight through the three months of experiments.

To my major professor, Dr. Alex. A. Volinsky, who encouraged me to transfer my degree to thesis-required degree, which gave me the opportunity to challenge myself, making my graduate study more meaningful.

To all my dear friends, who have always been by my side and made the two abroad years full of variety.

ACKNOWLEDGMENTS

I would first like to thank my thesis advisor Professor Alex. A. Volinsky of the College of Engineering at University of South Florida. He was always there whenever I ran into problems or had a question about my research or writing. He guided me to the right direction when he thought I needed it.

The author is grateful to Professor Kewei Gao and Professor Xiaolu Pang at the School of Materials Science & Engineering, the University of Science and Technology Beijing and their Ph.D. students: Chao Liu, Liang Wei, Qiufa Xu and Yanyun Bai. They all gave me a great help with my experiments.

This research was supported by NSF IRES 1358088 Program.

TABLE OF CONTENTS

LIST OF TABLES iii

LIST OF FIGURES iv

ABSTRACT... vi

CHAPTER 1: INTRODUCTION 1

CHAPTER 2: BEHAVIOR OF HYDROGEN IN METALS 4
2.1 Diffusion and Permeation of Hydrogen Through Metal 4
2.2 Hydrogen Flow Effects 5
2.2.1 The Effect of Metal Thickness 6
2.2.2 The Effect of Pressure 7
2.2.3 The Effect of Composition 7
2.2.4 The Effect of Tensile Stress 8
2.2.5 The Effect of Current Density 8
2.3 Hydrogen Embrittlement 8
2.3.1 Different Types of Hydrogen Embrittlement 9
2.3.1.1 Irreversible Hydrogen Embrittlement 9
2.3.1.2 Reversible Hydrogen Embrittlement 10
2.3.2 Impact Factors of Hydrogen Embrittlement 10
2.3.3 Prevention Techniques of Hydrogen Embrittlement 11
2.4 Effects of Hydrogen on the Mechanical Properties of Steel 11
2.4.1 Ductility 12
2.4.2 Tensile Strength 12
2.4.3 Impact Test 12
2.4.4 Conclusion of Hydrogen Effect on Mechanical Properties 13

CHAPTER 3: EFFECTS OF HYDROGEN ON THE TENSILE PROPERTIES OF THE X80 PIPELINE STEEL 14
3.1 Composition of X80 Steel 14
3.2 Mechanical Properties of X80 Steel 15
3.3 Hydrogen-charging Test 16
3.4 Slow Strain Rate Test (SSRT) 18
3.5 Results and Discussion 21
3.5.1 Stress-strain Curves 21
3.5.2 Relative Tensile Properties Loss 24

3.5.3 Surface Morphology of X80 Steel After SSRT....26
3.5.4 Lateral Fracture Morphology....28

CHAPTER 4: EFFECTS OF HYDROGEN ON THE CHARPY IMPACT TEST OF THE X80 PIPELINE STEEL....32
4.1 Experimental....32
4.2 Results and Discussion....35

CHAPTER 5: CONCLUSIONS AND FUTURE WORK....38
5.1 Conclusions....38
5.2 Future Work....39

REFERENCES....40

ABOUT THE AUTHOR....END PAGE

LIST OF TABLES

Table 1. Mechanical properties of the X80 steel. 15

Table 2. The experimental conditions used in this study 18

Table 3. Variation in mechanical properties of the X80 pipeline steels with different cathodic charging current densities 24

Table 4. Variation in mechanical properties of the X80 pipeline steels with different strain rates 25

Table 5. Results of X80 steel Charpy impact test 35

LIST OF FIGURES

Figure 1. Schematic diagram of the SSRT specimens used in this work.....15

Figure 2. Tensile specimen covered with silica gel 16

Figure 3. Schematic diagram of Slow Strain Rate Tensile test with dynamic hydrogen charging.....17

Figure 4. SSRT test with dynamic hydrogen charging equipment. 20

Figure 5. ZEISS Scanning Electron Microscope (SEM) used in this work. 20

Figure 6. Stress-strain curves of the X80 steel with constant strain rate and different current densities.. 21

Figure 7. Stress-strain curves of X80 steel with constant current density and different strain rates 22

Figure 8. Stress-strain curves of the X80 steel with different current densities under constant strain rate compared with uncharged samples at room temperature 23

Figure 9. Stress-strain curves of X80 steel with different strain rates under constant current density compared with uncharged samples at room temperature 23

Figure 10. The relative tensile strength loss of the X80 steel with different current densities 25

Figure 11. The relative tensile strength loss of the X80 steel with different strain rates 26

Figure 12. SEM fracture morphology of the X80 steel subjected to different hydrogen environments: (a) non-charged sample, (b) sample A-b, (c) sample B-b, and (d) sample C-b 27

Figure 13. The microcosmic SEM fracture morphology of the X80 steel subjected to different hydrogen environments: (a) non-charged sample, (b) sample A-b, (c) sample B-b, and (d) sample C-b. 28

Figure 14. SEM fracture morphology of the X80 steel subjected to different hydrogen environments: (a) non-charged sample, (b) sample B-a, (c) sample B-b, and (d) sample B-c 29

Figure 15. The microcosmic SEM fracture morphology of the X80 steel subjected to different hydrogen environments: (a) non-charged sample, (b) sample B-a, (c) sample B-b, and (d) sample B-c 29

Figure 16. SEM fracture lateral morphology of the X80 steel subjected to different hydrogen environments: (a) sample A-b, (b) sample B-b, (c) sample C-b.....30

Figure 17. SEM fracture lateral morphology of the X80 steel subjected to different hydrogen environments: (a) sample B-a, (b) sample B-b, (c) sample B-c.....31

Figure 18. Schematic diagram of impact specimens used in this work..... 32

Figure 19. Schematic diagram of static hydrogen charging of impact test sample 33

Figure 20. Sample of Charpy impact test, which is hydrogen charging in 0.1 mol/L NaOH solution.....34

Figure 21. Standard pendulum impact tester used in this work..... 34

Figure 22. Impact fracture morphology of X80 steel with different current densities (a) 0 mA/cm^2, (b) 2.53 mA/cm^2, (c) 4.60 mA/cm^2, (d) 6.03 mA/cm^2 36

Figure 23. Microcosmic impact fracture morphology of X80 steel with different current densities (a) 0 mA/cm^2, (b) 2.53 mA/cm^2, (c) 4.60 mA/cm^2, (d) 6.03 mA/cm^2. 37

ABSTRACT

The effect of hydrogen charging current density and tensile strain rate on the mechanical properties of X80 pipeline steel were investigated by slow strain rate test (SSRT), Charpy impact test, and scanning electron microscopy (SEM) in this thesis. The results show that both the ultimate tensile strength and elongation to failure of X80 steel were deteriorated significantly after charging with hydrogen. With a strain rate of 5 x 10^{-5} s^{-1}, the relative tensile strength and plasticity loss of X80 steel had no significant change within the range of assumed hydrogen partial pressures at room temperature. At room temperature, X80 steel had no apparent variation in ultimate tensile strength and elongation, except at the strain rate of 10^{-6} s^{-1}. Specimens obtained the greatest relative tensile strength loss and plasticity loss when strained at 10^{-6} s^{-1} with a current density of 4.6 mA/cm^2. The fracture morphology of two test groups of X80 steel exhibited significant brittle rupture when tested with dynamic hydrogen charging. The impact energy of X80 was not affected by hydrogen charging. Different current density also had no influence on the results of the impact test.

CHAPTER 1: INTRODUCTION

Due to the world economic recovery and the growing scale of the economic development of the developing countries, the energy and energy transportation has entered a state of extreme tension all over the world. In order to alleviate this situation, countries around the world started to develop new pipeline laying plan. Thus, worldwide pipeline steel demand is rising rapidly. At the same time, due to the increasing pipeline length, delivery pressure, and the deterioration of the environmental conditions along the pipeline, pipeline steels are expected to have better properties.

Pipeline is the most economical and reasonable transportation way for oil and natural gas. X80 high strength steel is one of the advanced pipeline steels that has been applied for many years for transporting natural gas since German Mannesmann Pipe steel company first successfully developed and laid a 3.2 km test line X80 steel in 1985. During 1992 and 1993, the company laid another 250 km gas pipeline, which has a thickness of 18.3 mm and 19.4 mm and delivery pressure of 10 MPa. This pipeline is still working well so far.

In China, X80 steel has been successfully applied in West-East Gas Pipeline Ⅱ, which is one of the natural gas pipelines. The pipeline runs from the western part of China to the east with a total length of 9,102 kilometers (5,656 mi), including 4,842 kilometers (3,009 mi) of the main line and eight sub-lines. [1] X80 pipeline steel is designed for service environment including seismic zones, landslides, and even tundra, etc. It can be said that X80 steel can be an excellent material for transporting natural gas. Lately, another gas transport line with similar laying path is

planned to be constructed in the future. The transmission medium, however, will change to synthetic natural gas (SNG) instead. Natural gas is substantially free of hydrogen, while SNG contains about 0.6% hydrogen. It is assumed that the partial pressure of hydrogen is 0.72 MPa. Prior research on X80 steel produced limited data on gaseous hydrogen under cathodic charging. The tensile behavior or mechanism of X80 steel in hydrogen environment has not been understood well. Therefore, studying the mechanical properties of X80 steel under the condition of new transport gas is vital for judging whether the X80 steel can be the material of the new pipeline.

When exposed to hydrogen gas environment, steels could suffer hydrogen damage or mechanical properties degradation. The penetrated hydrogen atoms diffuse into the steel and are trapped or precipitated at grain boundaries, dislocations and metallurgical defects, such as non-metallic inclusions, large precipitates, and bands of dense microstructure. [2, 3] Generally, hydrogen in steels is trapped into reversible and irreversible trap sites. [4] The amount of diffusible hydrogen is almost equivalent to the reversible hydrogen concentration in steels at room temperature. The individual hydrogen atoms within the metal gradually recombine to form hydrogen molecules, creating pressure from within the metal. This pressure can increase to levels, where the metal has reduced ductility, toughness, and tensile strength, up to the point where it cracks open. [5]

During the past decades, numerous studies focused on the hydrogen influence of temperate, [2, 3] strain rate [3, 4] and pressure [4, 6] on the mechanical properties of steel. Koichi Takasawa et al. [7] studied the effect of grain size on hydrogen embrittlement of high strength low alloy steel at 45 MPa of gaseous hydrogen. The results show that the grain refinement in high-pressure hydrogen could reduce the mass of hydrogen in unit grain boundary, so as to reduce the

hydrogen embrittlement susceptibility. M. Martin et al. [8] found that the yield and tensile strength were negligibly affected by the presence of hydrogen, whereas measurements of elongation to rupture and reduction of the area indicated an increasing ductility loss with decreasing austenite stability of the 304 austenitic stainless steel. Also, Walter et al. [9] investigated the influence of hydrogen pressure and notch severity on hydrogen embrittlement at ambient temperature, and found that embrittlement was shown to be a linear function of the square root of hydrogen pressure. Furthermore, embrittlement of low-alloy steels increased with stress concentration factor (Kt) at low Kt, passing through a maximum for Kt of 6 to 9, and then decreasing with Kt for higher Kt values. Boniszewski and Watkinson [10] clearly demonstrated, from extensive work on the heat-affected zone of welded steels, that hardness and microstructure are susceptible to hydrogen embrittlement. Huang et al. [11] studied the effects of microstructure and inclusions on the hydrogen induced crack susceptibility of X120 pipeline steel and concluded that the larger amount of inclusions contribute to hydrogen induced cracking of the steel.

On the other hand, few reports were about X80 steel. Also, no research or report about the hydrogen effects on the mechanical properties of X80 steel under the conditions of transporting SNG can be found. Therefore, it is necessary to conduct a special test for X80 steel and provide useful data to study the safety rules or make improvements in the future. Based on the former studies, this thesis is devoted to studying hydrogen behavior in steel and summarized impact factors of hydrogen in steel. Upon summary content and the new service environment, this thesis also conducted tensile and impact tests regarding uniform elongation, tensile strength, and impact energy of X80 pipeline steel. At the end of the thesis, evaluation was presented for applying the X80 steel in the new gas transportation line.

CHAPTER 2: BEHAVIOR OF HYDROGEN IN METALS

Metals often come into contact with hydrogen gas or hydrogen-producing environments. The influence of hydrogen on the properties of materials of construction is harmful, and sometimes calamitous. Understanding hydrogen behavior helps engineers study the mechanical properties degradation due to hydrogen embrittlement (HE). The hydrogen concentration in steel influences the degree of mechanical properties degradation. Hydrogen diffusivity influences crack propagation rate. Hydrogen absorption affects the amount and the rate of hydrogen entering steel. Thus, it is necessary for learning the characteristics of the metal-hydrogen system, to analyze the activities of hydrogen in metal phase, and to study the reaction mechanism of metal and hydrogen.

2.1 Diffusion and Permeation of Hydrogen Through Metal

At the metal surface, hydrogen molecules dissociate into atoms and adsorption of hydrogen atoms happens on the surface. Adsorbed atoms pass from the surface inside the metal with, possibly, a partial or total ionization of gas atoms and formation of new crystal phases of hydrides. [12] Inside of the metal phase, dissolved atoms or ions diffuse through the metal phase and pass its outgoing surface to desorb from the metal surface. Desorbed hydrogen atoms will then recombine into molecules.

The diffusion coefficient in solids is well predicted by the Arrhenius equation: [13]

$$D = D_0 e^{-E_A/(kT)} \quad (1)$$

where

D is the diffusion coefficient (m^2 / s),

D_0 is the maximum diffusion coefficient (at absolute temperature; m^2 / s),

E_A is the activation energy for diffusion with dimensions of (J $atom^{-1}$),

T is the absolute temperature (K),

k is the Boltzmann constant.

Equation 1 shows that diffusion coefficient is increasing with temperature. Taking the ln of both sides of Equation 1 yields:

$$\ln D = \ln D_0 - E_A/kT \quad (2)$$

Diffusion coefficient D is experimentally measured at a different temperature to draw the graph of $\ln D - 1/T$. The slope of the graph is used to calculate the activation energy E_A and the maximum diffusivity D_0. The hydrogen diffusion equation (Equation 1) can be therefore determined.

According to the Fick's second law [14] and its applicability to the flow of hydrogen through metals, the following approximate formula may be used for practical purposes:

$$x^2 = kDt \quad (3)$$

where x may be approximately assumed to be equal to the average penetration depth of the diffusion substance. The coefficient k in equation depends on the geometry of the sample; in this work, for a plate k = 4.

2.2 Hydrogen Flow Effects

Diffusion flux or the rate of hydrogen diffusion J, is commonly expressed in mol cm^{-2} sec^{-1} and for one dimensional planar diffusion is given by the Fick's first law: [14]

$$J = -D\frac{\delta C}{\delta x} \quad (4)$$

where $\frac{\delta C}{\delta x}$ is the concentration gradient along the *x*-coordinate, which is normal to the membrane surfaces. [15]

The flux of hydrogen can be obtained by converting the experimentally measured steady-state permeation current density *I* according to the following equation:

$$J = I/nF \quad (5)$$

The hydrogen permeation rate Φ (mol/cm s) is defined as:

$$\Phi = JL = LI/nF \quad (6)$$

where *n* is the number of transferred electrons, *F* is the Faraday's constant, and *L* (cm) is the specimen thickness.[16]

Many important factors affect the hydrogen flow in steel. Learning those factors may help people control the hydrogen environment of material to reduce hydrogen damage.

2.2.1 The Effect of Metal Thickness

The rate of diffusion, in conformity with the second Fick's law equation (Equation 3), should be inversely proportional to the metal thickness. In fact, this relation was confirmed by many studies. The reason thickness of the sample can affect diffusion coefficient and concentration is not very clear. One view is that it is due to the surface barrier layer. The other is that the thickness effect should cause by microvoids generated during cold working.

However, Heath [17], in his studies, suggests that the surface processes on both sides of the sample could cause deviation from the law of the inverse proportionality.

The surface layers of the cathode become supersaturated with hydrogen to a high concentration corresponding to a hypothetical "beta phase". The most probable reason is that the passage of hydrogen through that supersaturated layer is controlled by the processes of formation

and decomposition of the "beta phase", and not by the diffusion. In the case of thick membranes, the influence of these layers has an apparently less significant effect on the resulting rate of flow.

2.2.2 The Effect of Pressure

When a gas is forced through a wall made of porous material, the rate of the gas passage is directly proportional to the difference of gas pressure, or to the difference in the number of gas molecules striking both the surface of the wall per unit time. [15] From Smithells and Ransley, [18] the following equation represents the permeation rate Φ of hydrogen at low pressure when the partial pressure of hydrogen is p:

$$\Phi = \Theta k p^{\frac{1}{2}} \qquad (7)$$

here, Θ is the fraction of the surface covered by adsorbed gas atoms, and k is a proportionality factor.

2.2.3 The Effect of Composition

As pointed out by Smithells [19], of all the common metals α-iron shows maximum hydrogen permeability at 0 ℃; but some alloys of iron still have greater permeability. Bardenheuer and Thanheiser discovered in 1929 that the presence of carbon and the structural form of cementite in metals substantially diminish and influence the hydrogen permeation rate. Some investigators do not agree with it so far, as there is no precise data regarding the relation between diffusion values and carbon content and structure.

It is believed that the microstructure also has an effect on permeability. Amioit suggests that the martensite has the minimum permeability; spheroidal pearlite or fine pearlite has the maximum permeability. [20] Riecke [21] also concluded that the permeability of martensite or bainite structure is the lowest, and the permeability of pearlite and high-temperature tempered martensite is the highest. Further study shows that the size of carbides of tempered martensite did

not affect the permeability. When the decarburization makes C ≤ 5 wppm, the permeation rate of tempered martensite has the same value as of high temperature tempered martensite permeability. This shows that in the tempered martensite, carbide particles have no apparent effect on rate permeation rate of hydrogen. Permeability decreasing may be the effect of alloying elements. The small permeability of martensite structure may be related to the high internal stress.

2.2.4 The Effect of Tensile Stress

Danford [22] from NASA carried out the study concerning the influence of tensile stress on hydrogen diffusion in metal alloys. The results of the report show no significant trends in values of the hydrogen diffusion coefficients, which is in agreement with the results of Bockris et al. [23]. In the report of Bockris et al., hydrogen permeation of Armco iron and 4340 steel was increased by tensile stress with the hydrogen diffusion coefficient being unaffected by the applied stress.

2.2.5 The Effect of Current Density

The relationship between steady-state hydrogen flux *J* and steady-state current density *I* is shown in Equation 5. Hydrogen flux increases with the increasing current density until the hydrogen charging current density exceed the critical value. Current density should not be too large. Otherwise, it is easy to produce hydrogen bubbles, microcracks and other irreversible hydrogen damage on the surface of the specimen.

2.3 Hydrogen Embrittlement

Embrittlement is the process of losing of ductility of a material or making it brittle due to hydrogen absorption. A tiny amount of hydrogen could embrittle steels. [24] Hydrogen embrittlement is more susceptible to high strength steel with an ultimate tensile strength of more than 1000 MPa. [25]

2.3.1 Different Types of Hydrogen Embrittlement

2.3.1.1 Irreversible Hydrogen Embrittlement

Once irreversible hydrogen embrittlement occurs, the resulting plastic losses cannot recover by medium or room temperature hydrogen-relief treatment. Three main performances are demonstrated as following.

1) Hydrogen-Induced Cracking

In the material of some defect locations, H combined into H_2, and it is an irreversible reaction at room temperature that is H_2 will not be decomposed into H. With the increase of hydrogen concentration diffused into the defect, the pressure of the compound H_2 is also increased. Local plastic deformation will occur when the hydrogen pressure is greater than the yield strength. If the defect is on the sample surface, the surface will be summoned to form a hydrogen bubble, which is called Hydrogen-Induced Blistering (HIB). [26, 27]

When the hydrogen pressure is equal to the atomic bonding force, a microcrack will be generated, called Hydrogen-Induced Cracking (HIC). HIC includes steal flakes, H2S immersion crack, welding cold crack and microcrack produced under high fugacity condition. [28]

2) Hydrogen Corrosion

After applied at the high temperature and high-pressure hydrogen environment for a long time, high-pressure hydrogen and carbon will generate methane at the grain boundary in the steel. The generated CH_4 cannot spread out and form a bubble at the grain boundary inclusions. With the continuous formation of methane, methane pressure is greater than the strength of the material. So the bubble will transform into a crack, which embrittles the material. [29]

3) Cracking from Hydride Formation

Ti, Zr, Hf, V, Nb, Ta or rare earth and alkaline rare metals would like to form hydrides when the hydrogen concentration exceeds a certain level. The hydrides will decrease the ductility of the steel due to its typical low density and brittle compounds. [30]

2.3.1.2 Reversible Hydrogen Embrittlement

In the case of reversible embrittlement, ductility can be restored to steel as results of desorption of dissolved hydrogen, particularly at the elevated temperature. Fracture occurs without any signs of chemical reactions, microstructural changes, transformations, and damages, which is not connected with deformation. [31]

Kolachev [32] believed reversible hydrogen embrittlement is considered to be "true" hydrogen embrittlement and is one of the most complex phenomena associated with the effect of hydrogen on the mechanical and operating characteristics of metals.

Reversible HE results when three independent conditions occur simultaneously, a crack susceptible microstructure as the cause, the stress acting on the material and hydrogen environment as the triggers. If one or more of the conditions were removed or reduced below a critical value, hydrogen cracking would not occur. The exact mechanism of reversible hydrogen embrittlement is not well known yet. Most of the proposed mechanisms were based on slip interference by dissolved hydrogen near dislocation sites or microvoids. [33]

2.3.2 Impact Factors of Hydrogen Embrittlement

With certain hydrogen content, both the destruction degree of hydrogen and the incidence of embrittlement at room temperature tend to increase when strain rate decrease. Increasing temperature will reduce and even vanish cracks after heating to 200 °C. At high temperatures, hydrogen has a sufficient period to be driven out of solid solution. For steels that charged with

high hydrogen content during solidification, planar pressure theory is held to be an efficient mechanism. When hydrogen containing saturated steel is cooled at high temperature, the gaseous hydrogen in the microvoids will condense, and then develop into high-pressure hydrogen gas. This mechanism appears to apply only to the hydrogen-charged steel, not to steel in a low-pressure hydrogen environment. In the environment of low-pressure hydrogen, it is almost impossible to generate high pressure in solid. [24]

2.3.3 Prevention Techniques of Hydrogen Embrittlement

Hydrogen may be introduced into steel during melting and entrapped during solidification. Corrosion, hydrogen gas welding, and moisture also cause hydrogen embrittlement. Minimizing contact between the metal and hydrogen is the key to the embrittlement prevention techniques. Following are specific methods to prevent embrittlement.

- Reduce corrosion rate by inhibitor additions to decrease hydrogen pickup.
- Use clean steel with less number of voids to increase the resistance to hydrogen interstitials for embrittlement.
- Remove hydrogen by baking steel at 200-300 F to reverse hydrogen embrittlement.
- Conduct proper welding and maintain dry conditions since water and water vapor are major sources of hydrogen.
- Substitute elements such as Ni or Mo could make steel have very low hydrogen diffusion rates.

2.4 Effects of Hydrogen on the Mechanical Properties of Steel

Hydrogen and hydrogen producing environments have a harmful impact on the mechanical properties of steel, especially on its ductility. Experimental investigations about how hydrogen influences mechanical properties of steel have been going on for a long time. Valuable results,

which may allow drawing clear conclusions, have been obtained and reported in the literature. For instance, due to the actual presence of hydrogen within the metal, the action of hydrogen may both be direct and indirect. As another example, secondary effects, such as decarburization, cold working, the formation of voids, cracks, and notches, will affect the results of mechanical experiments. The effects of hydrogen on the mechanical properties will be discussed in the following sections.

2.4.1 Ductility

Ludwik [34] found considerable changes both in elongation and, particularly, in the reduction of fracture values in mild steel specimens after pickling in 2.5% sulphuric acid. [16]

Comparing the effect of hydrogenation of low alloy steels on the reduction in area at fracture, Hobson and Hewitt, [35] Bastien and Amiot (1954), Amiot [36] and Skluev et al. [37] concluded that the higher the tensile strength of the steel, the greater was the degree of embrittlement. However at equal tensile strength values, different susceptibilities were observed, depending on the structure of the steel. Also, the less susceptible are steels to the effect of hydrogen; the greater is the ductility of the given steel, and the closer is its actual state to the state of physical-chemical, structural and mechanical equilibrium.

2.4.2 Tensile Strength

Usually, the tensile strength is unaffected or at most only slightly affected by the presence of hydrogen. On the other hand, the ultimate tensile strength, which is connected with the ductility, is considerably lowered by hydrogenation.

2.4.3 Impact Test

The majority of impact test results showed that only little effects of hydrogenation are to be observed on the impact strength of steel. It is because the impact test involves high deformation

rates. However, Hobson and Sykes emphasize that since the impact strength depends to a large extent on crack initiation at the surface of the test specimen, and hydrogen quickly escapes from this surface layer, the results of impact test may underestimate the true effect of hydrogen on notch brittleness.

2.4.4 Conclusion of Hydrogen Effect on Mechanical Properties

In conclusion, hydrogen greatly influences the plastic properties, but this effect disappears at low temperatures and high deformation rates. However, neither by cooling the steel nor by increasing the deformation rate, the embrittlement of steel cannot be removed at high hydrogen concentrations. So far, there have been no proposed mechanisms of hydrogen embrittlement, which can explain all the observed effects.

CHAPTER 3: EFFECTS OF HYDROGEN ON THE TENSILE PROPERTIES OF THE X80 PIPELINE STEEL

Tensile test is often used to study the influence of hydrogen on mechanical properties, in which a specimen is loaded in uniaxial tension until failure. Based on the service environment of the X80 steel, which has been discussed in the introduction section, samples will be charged with hydrogen under different current density to simulate different delivery pressure before being tested. The effects of strain rate will also be tested for certain current density. All experiments were performed at room temperature. To ensure the reliability of the experimental data, each test was repeated at least three times.

3.1 Composition of X80 Steel

X80 steel is a widely used natural gas pipeline. Its high strength is a result of combining ferrite and bainite microstructure of dual-phase steel. The ferrite phase gives X80 steel low initial yield stress and high ductility, and the bainite provides high ultimate tensile strength. The combination of high strength and elongation makes X80 steel an ideal material for bearing large deformation without failing.

The X80 pipeline steel studied in this research has a chemical composition (wt.%): C 0.07, Mn 1.86, Si 0.27, Cr 0.04, Mo 0.3, Cu 0.27, Al 0.026, S 0.01, P 0.015, Ti 0.01, Nb 0.079, and Fe balance. The carbon content of X80 steel is typically 0.04 % ~ 0.08 %. Reducing carbon content of steel will decrease the yield strength, which could be compensated by another strengthening mechanism. The most common way is to substitute Mn for C. The added Mn not only increases

the solid solution but also improves the strength, toughness as well as the ductility of the material. Increased Mn content will accelerate the central segregation of controlled rolling steel plate. Therefore, the addition range of Mn in steel is generally from 1.1% to 2% according to the different requirements of plate thickness and strength. [38]

3.2 Mechanical Properties of X80 Steel

Before being tested, all the specimens were manually 2000 grit carbid silicon paper to clean the sample surface and to generate similar roughness. They were then degreased with acetone and blow-dried. Tensile properties were obtained using LETRY slow strain tensile test machine. Dimensions of specimens are shown in Figure 1. Tensile tests were performed at 27 °C and a rate of 3 x 10^{-3} s^{-1}. Toughness characteristics were measured at -10 °C by using the Charpy-V notch test. Results are summarized in Table 1.

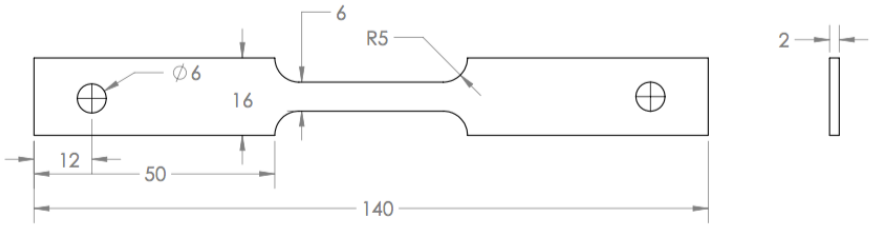

Figure 1. Schematic diagram of the SSRT specimens used in this work. Dimensions are in mm.

Table 1. Mechanical properties of the X80 steel.

UTS (MPa)	El %	Charpy-V (-10 °C, J)
708±13.6%	19.3±0.83%	223±8.7%

3.3 Hydrogen-charging Test

Flat tensile specimens having a 30 mm gauge length, 6 mm gauge width and 2 mm thick were oriented with their major axes parallel to the longitudinal axes of the pipes. The gauge length was manually ground with 2000 grit SiC paper and polished to a fine finish with 1.2 μm diamond paste. Welded the sample with a wire and covered it with silica gel except the gauge length to protect the samples from hydrogen, shown in Figure 2.

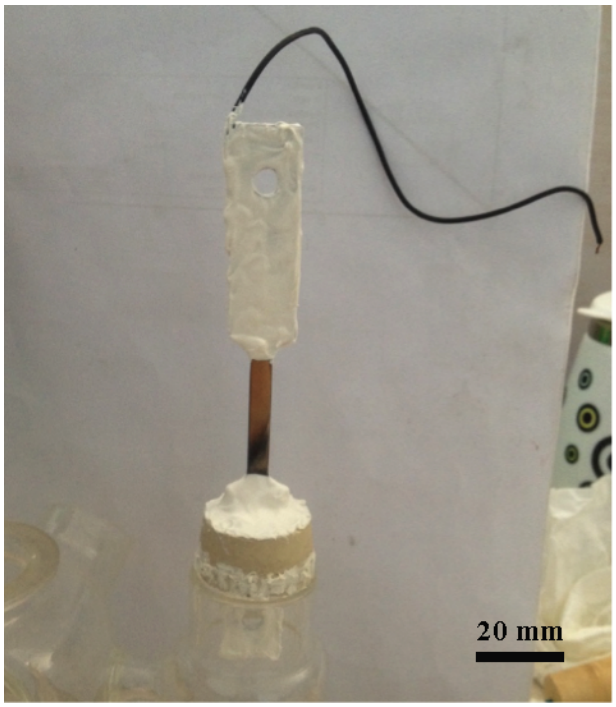

Figure 2. Tensile specimen covered with silica gel.

During hydrogen charging, the steel was immersed in 0.1 mol/L NaOH solution at room temperature, with various cathodic charging current densities of 2.53 mA/cm^2, 4.60 mA/cm^2 and 6.03 mA/cm^2, respectively. These current densities were chosen to most closely simulate hydrogen partial pressure in buried pipe (0.72 MPa). From Kumnick et al. [39], the relation between current density i (mA/cm^2) and pressure p (MPa) is

$$\sqrt{p} = 0.15798i + 0.04777 \quad (8)$$

Using 0.2 MPa, 0.6 MPa and 1.0 MPa as p values, the forenamed charging densities will be solved for.

While charging, reaction on cathode steel is,

$$H^+ + e \rightarrow H \quad (9)$$

Because of the high concentration of H, some H recombined to H_2 on the surface of X80 steel, while others diffused into the steel.

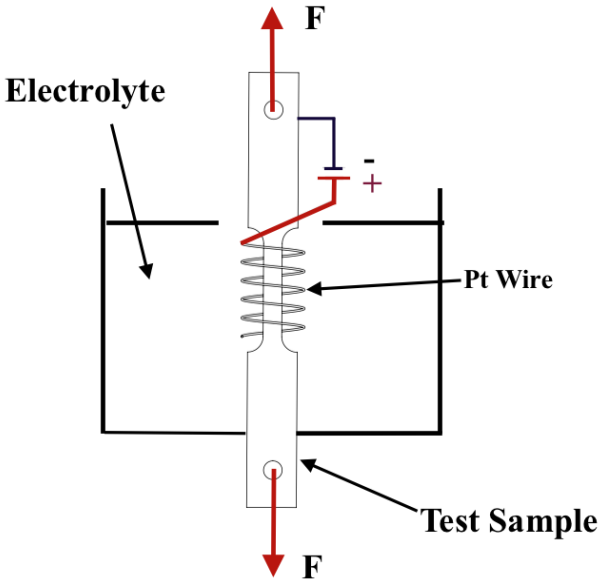

Figure 3. Schematic diagram of Slow Strain Rate Tensile test with dynamic hydrogen charging.

All specimens were pre-charged for one hour before tensile tests and kept charging during slow strain rate tensile tests. The static hydrogen charging before testing was carried out in 0.1 mol/L NaOH solution with a cathodic current density of 4.6 mA/cm^2. The illustration of the equipment for the dynamic hydrogen charging is shown in Figure 3. The dynamic hydrogen charging started as soon as yielding occurred during tensile testing. Various cathodic current

densities were used to change the amount of dissolved hydrogen in specimens. When the current density and charging time increased to a critical value, the surface of the specimen will cover with some pitting corrosion, which will affect the mechanical properties of steel. So, it is necessary to select the appropriate charging density and time for hydrogen pre-charging before dynamic hydrogen charging.

Yield stress, ultimate tensile strength and the elongation before and after charging were compared to assess the effects of hydrogen

3.4 Slow Strain Rate Test (SSRT)

To investigate the effect of strain rate and partial pressure separately, slow strain rate tensile tests were first conducted at a strain rate of 5 x 10^{-6} s^{-1} with various current densities of 2.53 mA/cm^2, 4.6 mA/cm^2, and 6.03 mA/cm^2, respectively. Tests were then carried out at different strain rates of 10^{-5} s^{-1}, 5 x 10^{-6} s^{-1} and 10^{-6} s^{-1} with a current density of 4.6 mA/cm^2, respectively, on a slow strain rate test system (LETRY) at room temperature. Strain rates in the 10^{-5} s^{-1} to 10^{-6} s^{-1} range are used for numerous material-environment systems. For convenience, these current densities were named A, B and C, and the strain rate as a, b and c. Table 2 gives the detailed experimental conditions.

Table 2. The experimental conditions used in this study.

Conditions	Current density (mA/cm^2)	Strain rate (s^{-1})
A-b	2.53	5 x 10^{-6}
B-b	4.6	5 x 10^{-6}
C-b	6.03	5 x 10^{-6}
B-a	4.6	1 x 10^{-5}
B-c	4.6	1 x 10^{-6}

The sample was placed in the SSRT system in a container with 0.1 mol/L NaOH. Therefore, tensile tests can be conducted while charging with hydrogen. The sample will then be strained to failure and stress-strain curves will be plotted to calculate the yield stress and ultimate tensile strength. The relative tensile strength loss I_σ (RTSL) and relative plasticity loss I_δ (RPL), shown in Equations 10 and 11, were used to determine the relative susceptibility to hydrogen damage. [40]

$$I_\sigma(\%) = \frac{\sigma_0 - \sigma_H}{\sigma_0} \times 100\% \quad (10)$$

$$I_\delta(\%) = \frac{\delta_0 - \delta_H}{\delta_0} \times 100\% \quad (11)$$

where σ_0 and δ_0 are the ultimate tensile strength and elongation to failure without hydrogen charging, and σ_H and δ_H are the ultimate tensile strength and elongation to failure after hydrogen charging. After the tensile tests, the fracture surfaces of the specimens were subjected to a detailed analysis via scanning electron microscopy (SEM).

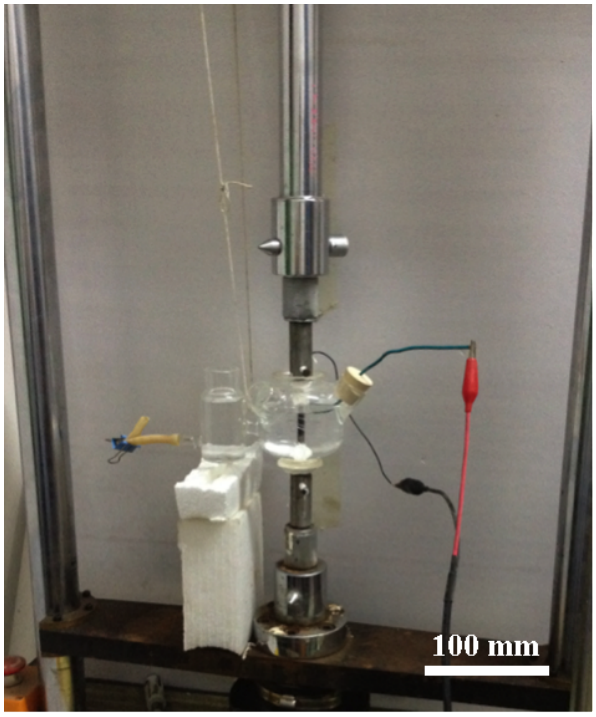

Figure 4. SSRT test with dynamic hydrogen charging equipment.

Figure 5. ZEISS Scanning Electron Microscope (SEM) used in this work.

3.5 Results and Discussion

3.5.1 Stress-strain Curves

The stress-strain curves for each test conditions were obtained from SSRT tests shown in Figure 6 and Figure 7. The variation of stress-strain curves is relatively stable in each test condition. However, all stress-strain curves of specimens with hydrogen charging look more like brittle materials than ductile materials. Especially in Figure 6a and Figure 7c, sample A-b and sample B-c do not have yield points, and do not strain-harden, which are typical characters of stress-strain curves for brittle materials.

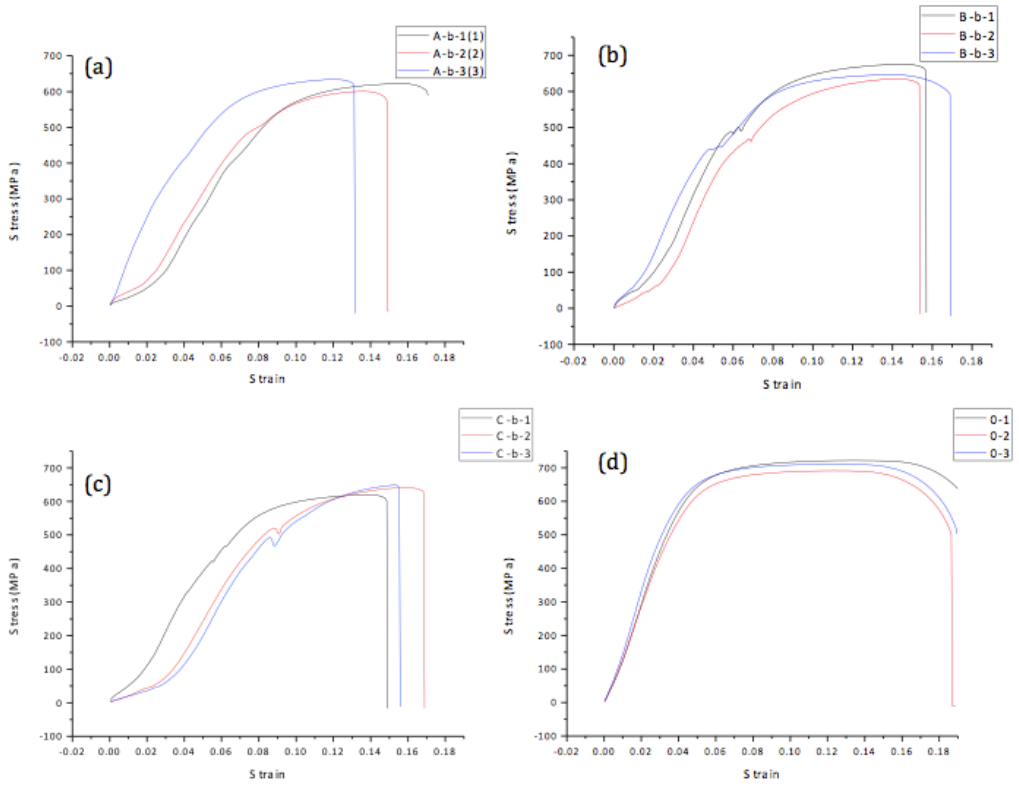

Figure 6. Stress-strain curves of the X80 steel with constant strain rate and differernt current densities. Rates of (a), (b), (c) 5 x 10^{-6} s^{-1}; (d) 0.2 s^{-1} and current densities of (a) 2.53 mA/cm^2, (b) 4.60 mA/cm^2, (c) 6.03 mA/cm^2, (d) 0 mA/cm^2 at room temperature.

Figure 8 shows the stress-strain curves of the X80 steel measured at different current densities under constant strain rate and compared with uncharged samples. All chosen samples

were typical specimens from each test condition. It can be seen that the tensile strength, toughness and elongation to failure of the X80 steel all had a significant loss in hydrogen environment. UTS and toughness increase a little with the rise of hydrogen charging current density.

In Figure 9, sample B-c-2 has the lowest tensile strength and strain at fracture, while the other two samples are holding similar results. Detailed analysis will be discussed, using specific experimental data. The degradation of fracture toughness decreases with the increasing H_2 pressure. However, the simulated hydrogen partial pressures in this test do not have enough difference to a significantly influence X80 steel.

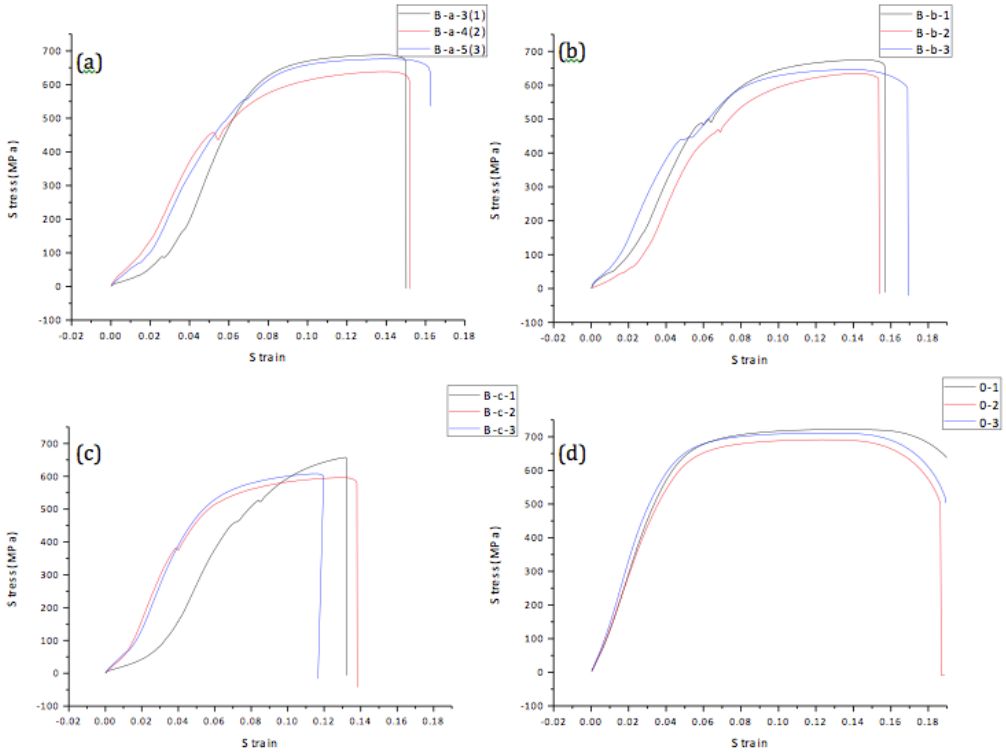

Figure 7. Stress-strain curves of X80 steel with constant current density and different strain rates. Current density of (a), (b), (c) 4.60 mA/cm^2; (d) 0 mA/cm^2 and strain rates of (a) 1 x 10^{-5} s^{-1}, (b) 5 x 10^{-6} s^{-1}, (c) 1 x 10^{-6} s^{-1}, (d) 3 x 10^{-3} s^{-1} at room temperature.

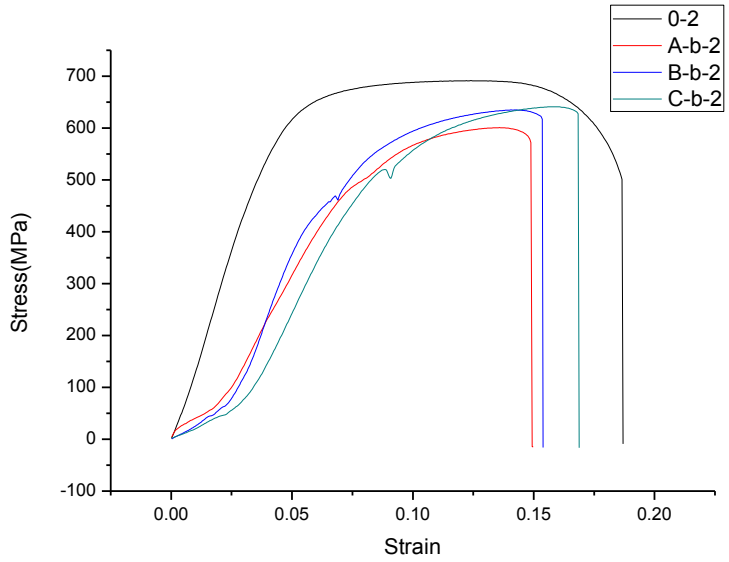

Figure 8. Stress-strain curves of the X80 steel with different current densities under constant strain rate compared with uncharged samples at room temperature.

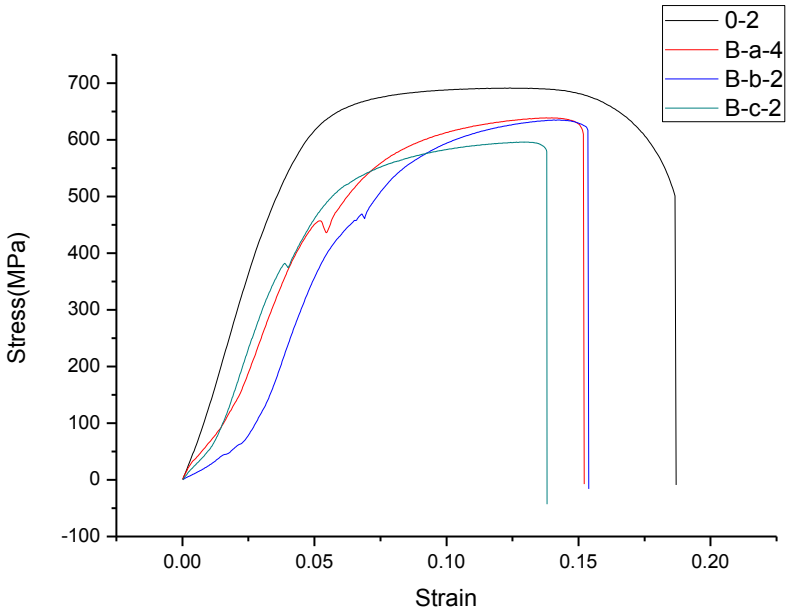

Figure 9. Stress-strain curves of X80 steel with different strain rates under constant current density compared with uncharged samples at room temperature.

3.5.2 Relative Tensile Properties Loss

It can be seen from Table 1, Table 3 and Table 4, there was a significant loss in ductility in all test groups when tested after cathodic charging. Ductility can be quantified by the elongation and by the reduction of area at fracture. Under constant strain rate (Table 3), however, the ultimate tensile strength and elongation of samples had nearly no change with the increase of current density. As displayed in Table 4, there was no apparent difference in the tensile properties results of specimens tested at B-a and B-c conditions. It can be deduced that the effect of hydrogen on hydrogen embrittlement of X80 steel remains unchanged within the range of strain rate from 1 x 10^{-5} s^{-1} to 5 x 10^{-6} s^{-1}. This analysis can be confirmed by the results shown in Figure 11. At a slow strain rate of 1 x 10^{-6} s^{-1}, on the other hand, which lengthened the failure time and hydrogen charging time of samples, the UTS of X80 steel had a slight reduction and meanwhile samples had a significant loss in elongation.

To further analyze the damage of hydrogen on tensile properties, the relative tensile strength loss and the relative plasticity loss of the X80 steel under constant strain rate and current density are shown in Figure 10 and Figure 11, respectively. Dynamic hydrogen charging specimens shows a slight drop in tensile strength with an increase in the charging current density.

Table 3. Variation in mechanical properties of the X80 pipeline steels with different cathodic charging current densities.

Specimens	Current density (mA/cm^2)	UTS (MPa)	Average UTS (MPa)	Elongation %	Average elongation %	Time to failure (h)
A-b-1	2.53	622	619±13.6%	17	15±1.6 %	9.6
A-b-2		601		14.9		8.4
A-b-3		634		13.2		7.4
B-b-1	4.60	675	652±16.8%	15.7	16±0.6 %	8.9
B-b-2		635		15.4		8.7
B-b-3		647		16.9		9.6
C-b-1	6.03	620	636±16.9%	14.9	15.7±0.8 %	8.4
C-b-2		641		16.8		9.5
C-b-3		648		15.5		8.8

Table 4. Variation in mechanical properties of the X80 pipeline steels with different strain rates.

Specimens	Strain rate (s^{-1})	UTS (MPa)	Average UTS (MPa)	Elongation %	Average elongation %	Time to failure (h)
B-a-3	1 x 10^{-5}	646	654±16.1%	15	15.5±0.6%	4.2
B-a-4		639		15.2		4.3
B-a-5		676		16.3		4.6
B-b-1	5 x 10^{-6}	675	652±16.8%	15.7	16±0.6%	8.9
B-b-2		635		15.4		8.7
B-b-3		647		16.9		9.6
B-c-1	1 x 10^{-6}	658	621±26.8%	13.2	13±0.7%	37.4
B-c-2		596		13.8		39.0
B-c-3		608		12		33.8

As illustrated in Figure 11, the relative plasticity loss of the tested steel is comparably significant for a very slow strain rate. However, a distinct change with the charging current density or tensile rate can be hardly found. In other words, all these samples appear to suffer a similar degree of embrittlement, expect at the lowest strain rate, where the level of embrittlement tends to increase a lot when extending the tensile time in the hydrogen environment.

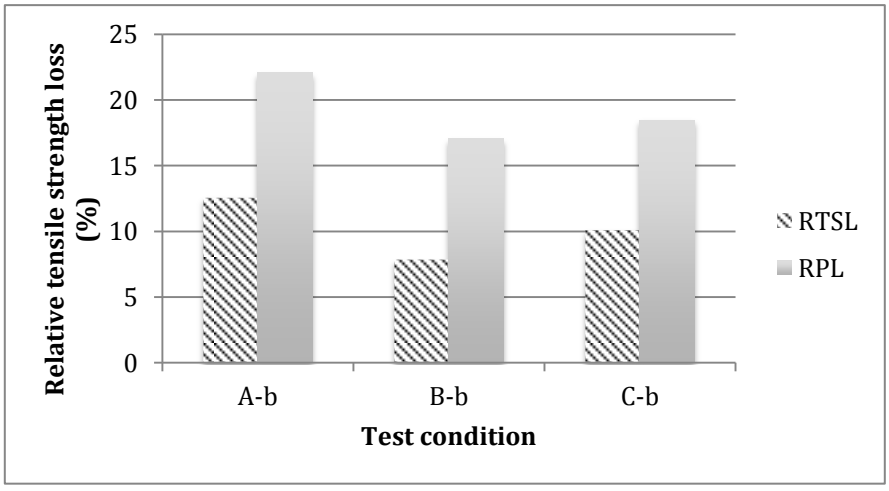

Figure 10. The relative tensile strength loss of the X80 steel with different current densities.

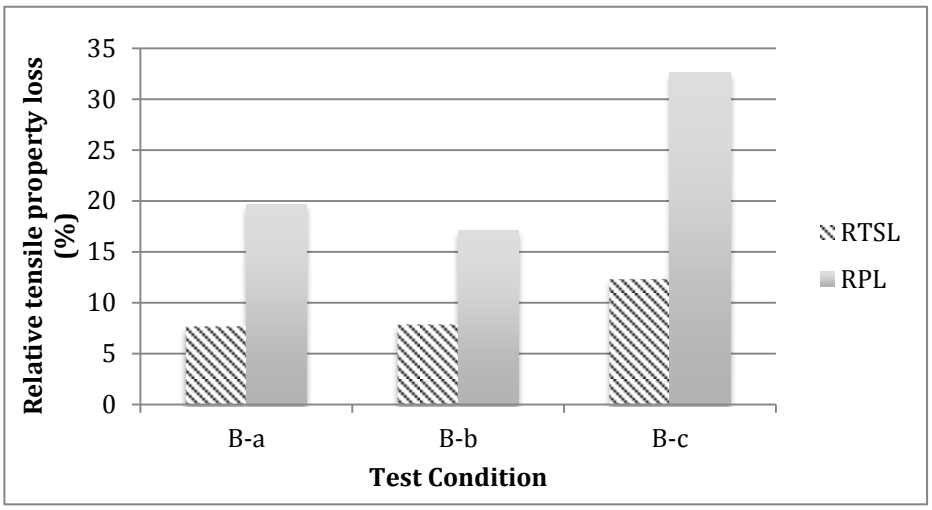

Figure 11. The relative tensile strength loss of the X80 steel with different strain rates.

For most steels, the susceptibility of hydrogen embrittlement is more severe with the ultimate tensile strength up to 1000 MPa. It may explain the fact that the degradation degree of tensile properties of X80 steel did not vary a lot with different hydrogen content. The significant decrease in elongation suggests that hydrogen embrittlement occurred in the steel.

All experimental results can be explained as the effects of hydrogen diffusion and hydrogen permeation in steel. Besides, combining the results of Table 3 and Table 4, it can be deduced that hydrogen charging current density and charging time are the key factors of influence on tensile properties.

3.5.3 Surface Morphology of X80 Steel After SSRT

Figure 12 and Figure 13 show the SEM morphology of the fracture surface of the X80 steel subjected to different hydrogen charging currents in comparison to the morphology of specimens fracture in air. As shown in Figure 12, the reduction of the area of the fracture surface of the uncharged specimen is significantly larger compared to other samples that fracture in the hydrogen environment. Those specimens strained after charging show almost no necking. This

indicated that the fracture of steel in hydrogen environment changed to brittle fracture. The reduction in ductility is a manifestation of damage done to the steel during the cathodic charging, which must also be attributed to the absorption of hydrogen during that process. [41] Besides the reduction of area, a 45° shear fracture surface was also observed from some charged samples.

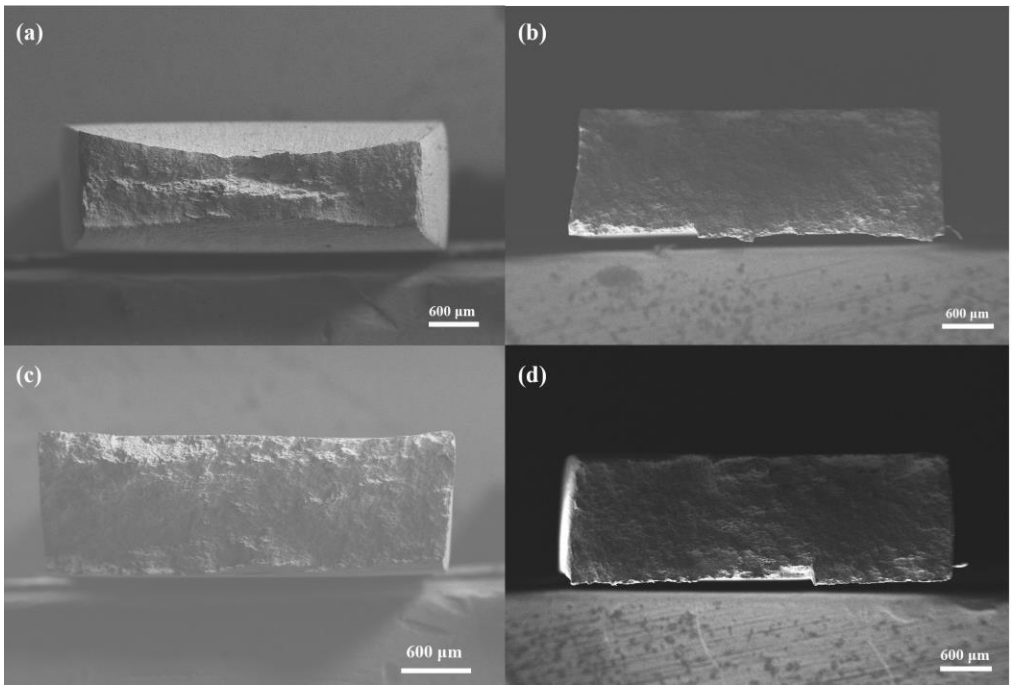

Figure 12. SEM fracture morphology of the X80 steel subjected to different hydrogen environments: (a) non-charged sample, (b) sample A-b, (c) sample B-b, and (d) sample C-b.

In SEM image in Figure 13, the fracture surface of the uncharged specimen shows many microvoids with a small range of sizes, including small and shallow dimples. For the hydrogen charged specimens, the fracture surfaces exhibit broad and deep dimples, which show better plasticity. In Figure 15, the fracture surface of the uncharged specimen shows many microvoids with a small range of sizes, including small and shallow dimples. For the hydrogen charged specimens, the fracture surfaces exhibit broad and deep dimples, which show better plasticity.

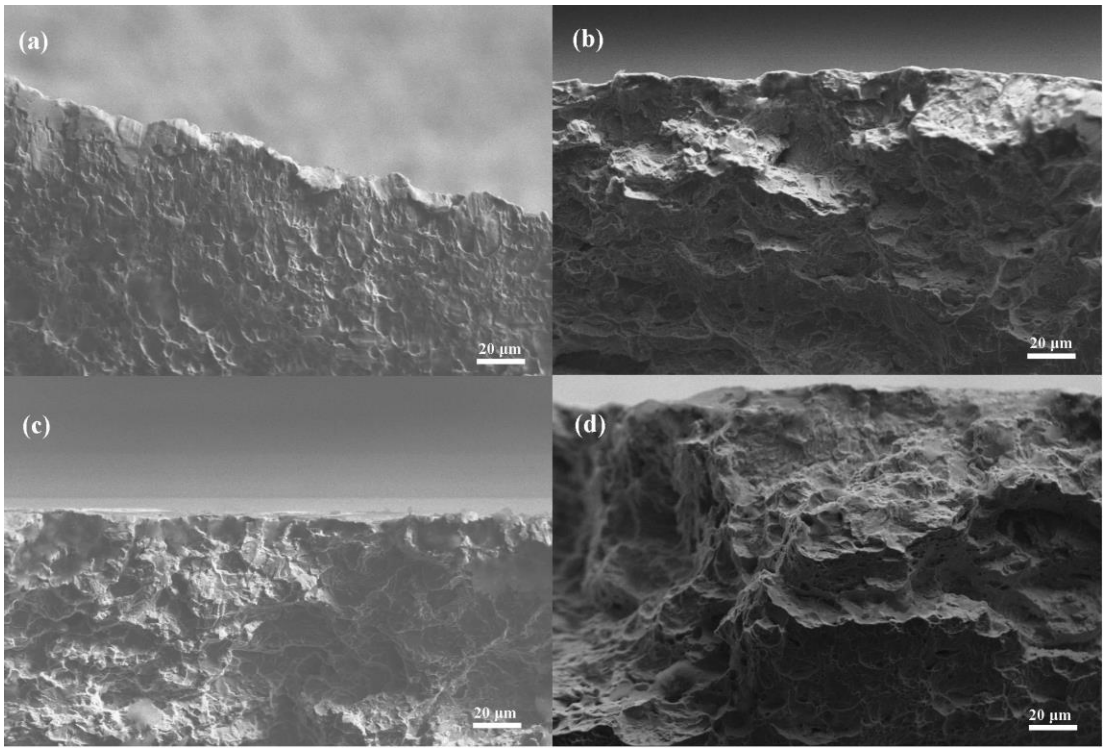

Figure 13. The microcosmic SEM fracture morphology of the X80 steel subjected to different hydrogen environments: (a) non-charged sample, (b) sample A-b, (c) sample B-b, and (d) sample C-b.

3.5.4 Lateral Fracture Morphology

Many small cracks and creep appeared on the surface of sample A-b. With increased current density, specimens were smoother with fewer cracks and creep were seen on the fracture surface. Sample C-b almost had no creep near fracture.

A similar phenomenon was found in Figure 17. Greater strain rate has larger number of creep and cracks. No crack was found near fracture from sample B-c, where strain rate was 10^{-6} s^{-1} and current density is 4.6 mA/cm^2. As it known well, plastic deformation is a sign for ductile fracture. Cracks propagate near fracture area. After analyzing all the results of sample B-c, it can be concluded that X80 steel transferred to brittle material when strain with a rate of 10^{-6} s^{-1} and with a hydrogen partial pressure of 1 MPa.

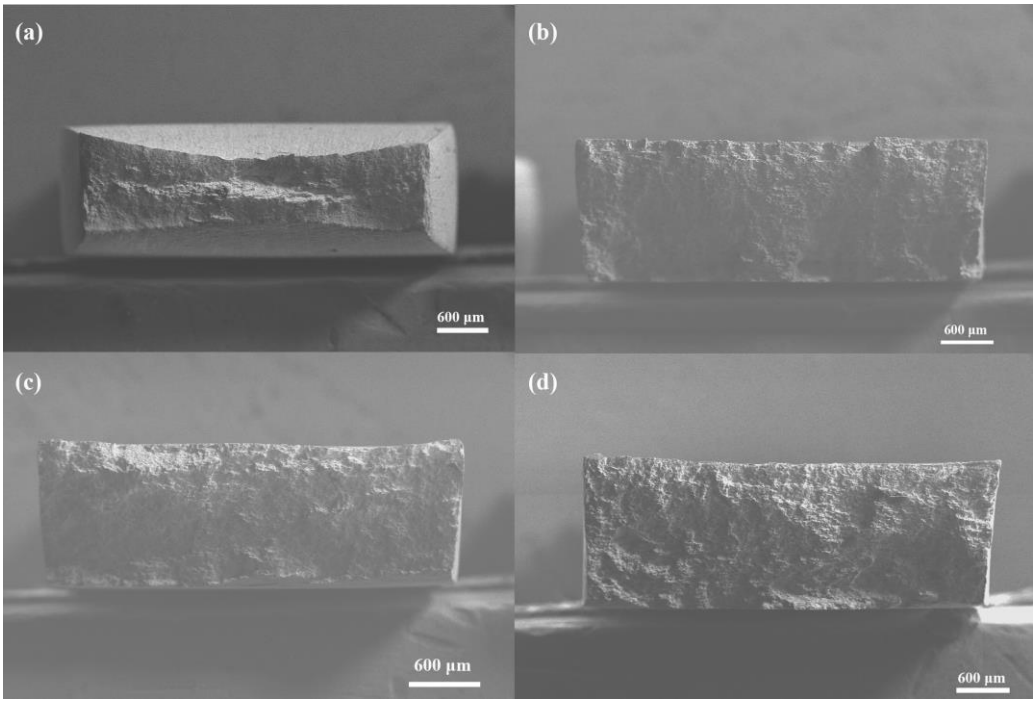

Figure 14. SEM fracture morphology of the X80 steel subjected to different hydrogen environments: (a) non-charged sample, (b) sample B-a, (c) sample B-b, and (d) sample B-c.

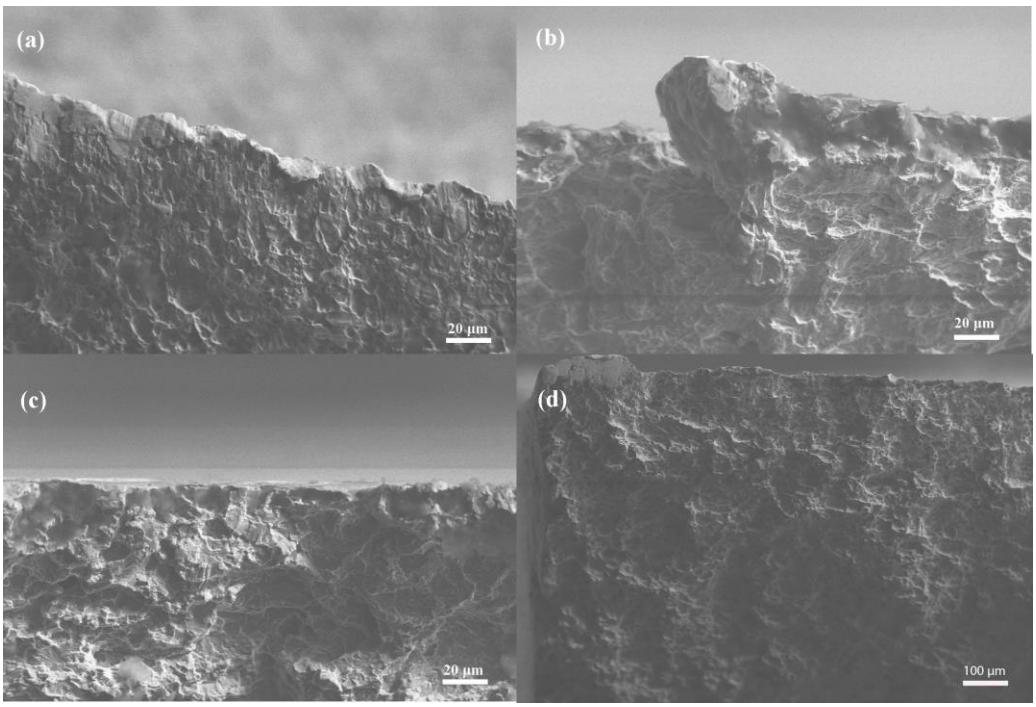

Figure 15. The microcosmic SEM fracture morphology of the X80 steel subjected to different hydrogen environments: (a) non-charged sample, (b) sample B-a, (c) sample B-b, and (d) sample B-c.

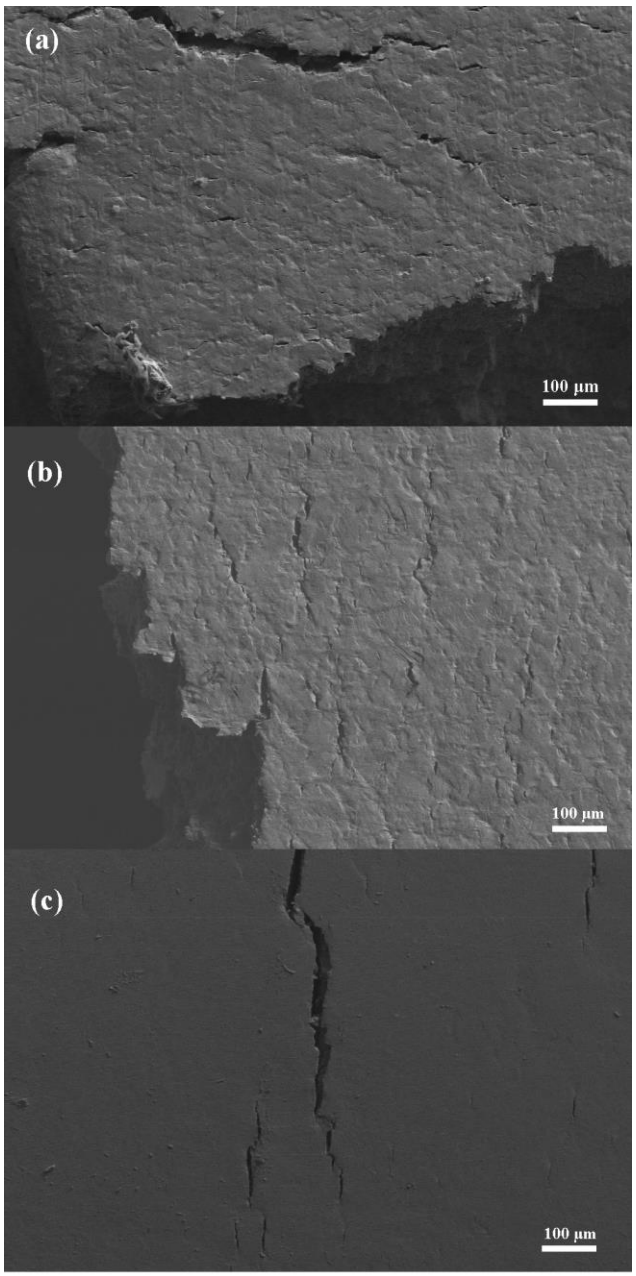

Figure 16. SEM fracture lateral morphology of the X80 steel subjected to different hydrogen environments: (a) sample A-b, (b) sample B-b, (c) sample C-b.

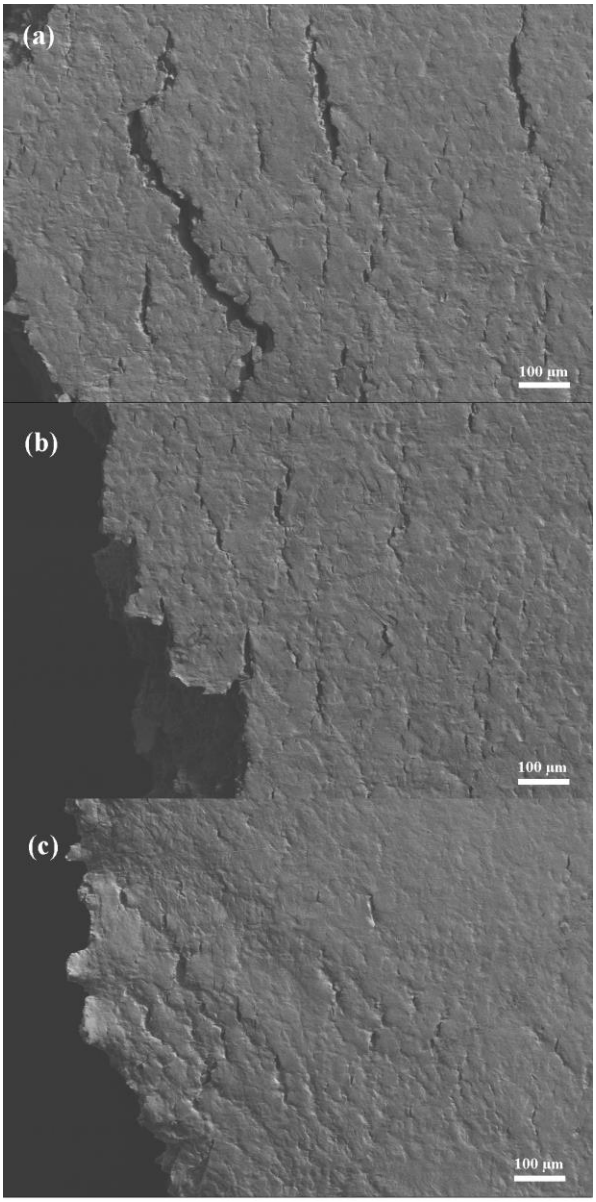

Figure 17. SEM fracture lateral morphology of the X80 steel subjected to different hydrogen environments: (a) sample B-a, (b) sample B-b, (c) sample B-c.

CHAPTER 4: EFFECTS OF HYDROGEN ON THE CHARPY IMPACT TEST OF THE X80 PIPELINE STEEL

4.1 Experimental

The Charpy impact test is the standardized method to determine the absorbed amount of energy by a material during fracture. The specimens, shown in Figure 18, were machined and tested on a 300J pendulum impact tester according to ASTM A370. [42] Specimens were ultrasonically cleaned with ethyl alcohol and blow-dried before charging.

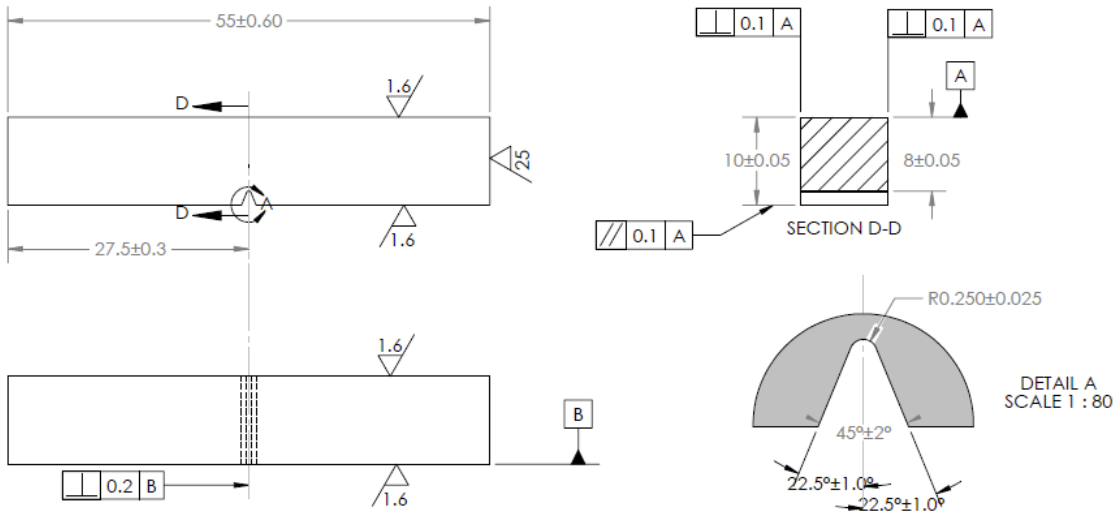

Figure 18. Schematic diagram of impact specimens used in this work.

At room temperature, all specimens were per-charged at least 24 h in 0.1 mol/L NaOH solution with current densities of A: 2.53 mA/cm^2; B: 4.60 mA/cm^2; C: 6.03 mA/cm^2. The

sample was charged as the cathode while platinum wire was the anode. Figure 19 and Figure 20 are the schematic and the actual figure of static hydrogen-charging impact sample in 0.1 mol/L NaOH solution, respectively.

After charging hydrogen, specimens were immediately preserved at -10 °C in liquid nitrogen for 10 minutes. Specimens were fractured in 2 seconds once removed from the liquid medium. The impact speed of the pendulum in Figure 21 would be 5 m/s to 5.5 m/s at the moment of impact. To ensure the reliability of the experimental data, each test was repeated at least three times.

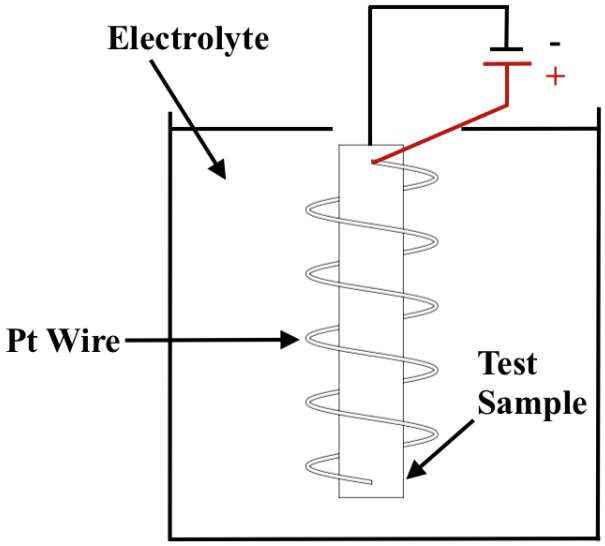

Figure 19. Schematic diagram of static hydrogen charging of impact test sample.

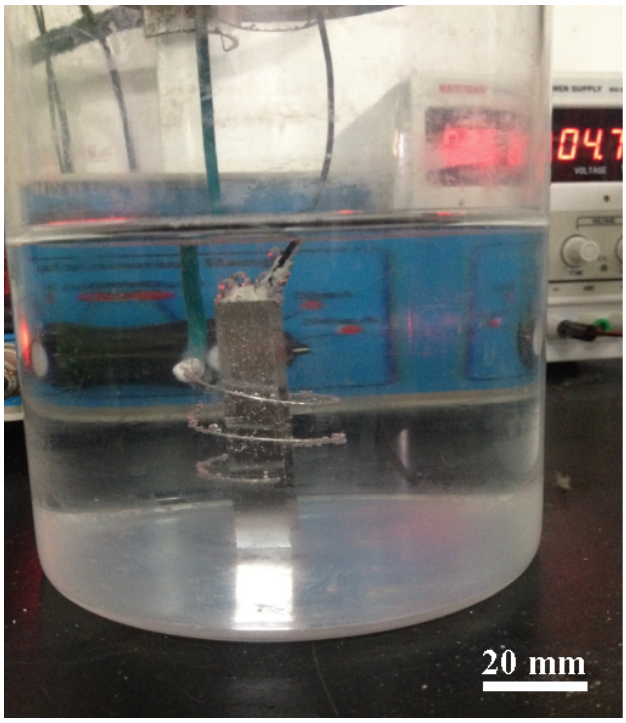

Figure 20. Sample of Charpy impact test, which is hydrogen charging in 0.1 mol/L NaOH solution.

Figure 21. Standard pendulum impact tester used in this work.

4.2 Results and Discussion

As discussed in Chapter 2.4.3, hydrogen does not significantly affect the impact test due to the high deformation rate for most of the materials. This conclusion also applies to X80 steel. The impact energy of uncharged specimen is 223±8.7% J. By comparing the results of uncharged specimens with the results shown in Table 5, it can be seen that the impact energy of X80 was not affected by hydrogen charging. Different current density also had no influence on the results of the impact test. A more scientific way to conclude this result is to calculate the p-value of the impact test results. *P*-value is widely used in null hypothesis significance testing to help tester quantify the idea of statistical significance of evidence. [43] An independent-samples t-test was used to check the influence of hydrogen charging on impact energy, p (12) = 0.242. Since $p \geq 0.05$, it is concluded that no significant difference between charged samples and uncharged samples was found.

Table 5. Results of X80 steel Charpy impact test.

Sample	Current density (mA/cm^2)	Impact energy (-10 ℃, J)
A	2.53	211.6±2.4%
B	4.60	235.7±6.9%
C	6.03	228.3±2.4%

Figure 22 is the fracture morphology of X80 steel after Charpy impact test. Uncharged impact sample had a flat smooth break surface with no stratification and not obvious radiation zone. The ductile region covered the entire section. The impact specimens after hydrogen charging had a small amount of stratification. No significant difference of the stratification was observed between different current densities charging samples. All charged samples show brittle

fracture characters. In Figure 23, there is the microscopic fracture morphology of X80 steel impact after 24 hours charging hydrogen with different current densities. The number and size of dimples of the uncharged sample seems the same as the charged samples. Also, the microstructure had no apparent change with the increase of current density. The observed results are explained in section 2.4.3. The impact strength depends to a large extent on crack initiation at the surface of the test specimen, and hydrogen quickly escapes from this surface layer. The results of impact test may underestimate the true effect of hydrogen on notch brittleness.

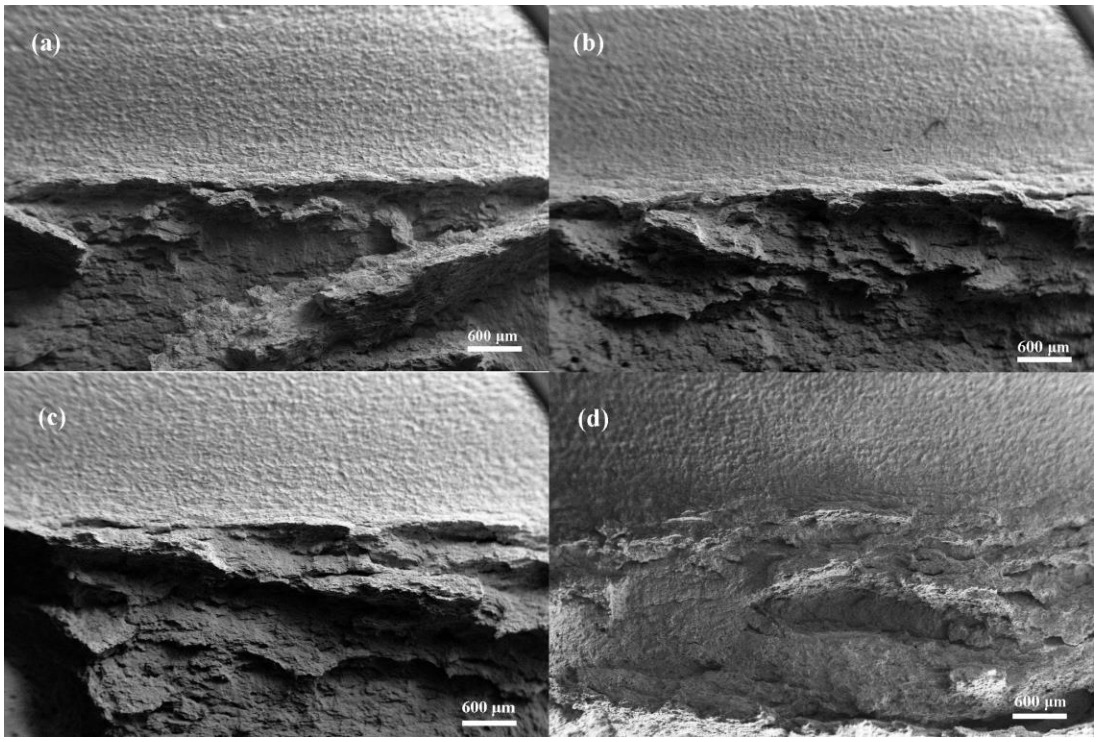

Figure 22. Impact fracture morphology of X80 steel with different current densities (a) 0 mA/cm^2, (b) 2.53 mA/cm^2, (c) 4.60 mA/cm^2, (d) 6.03 mA/cm^2.

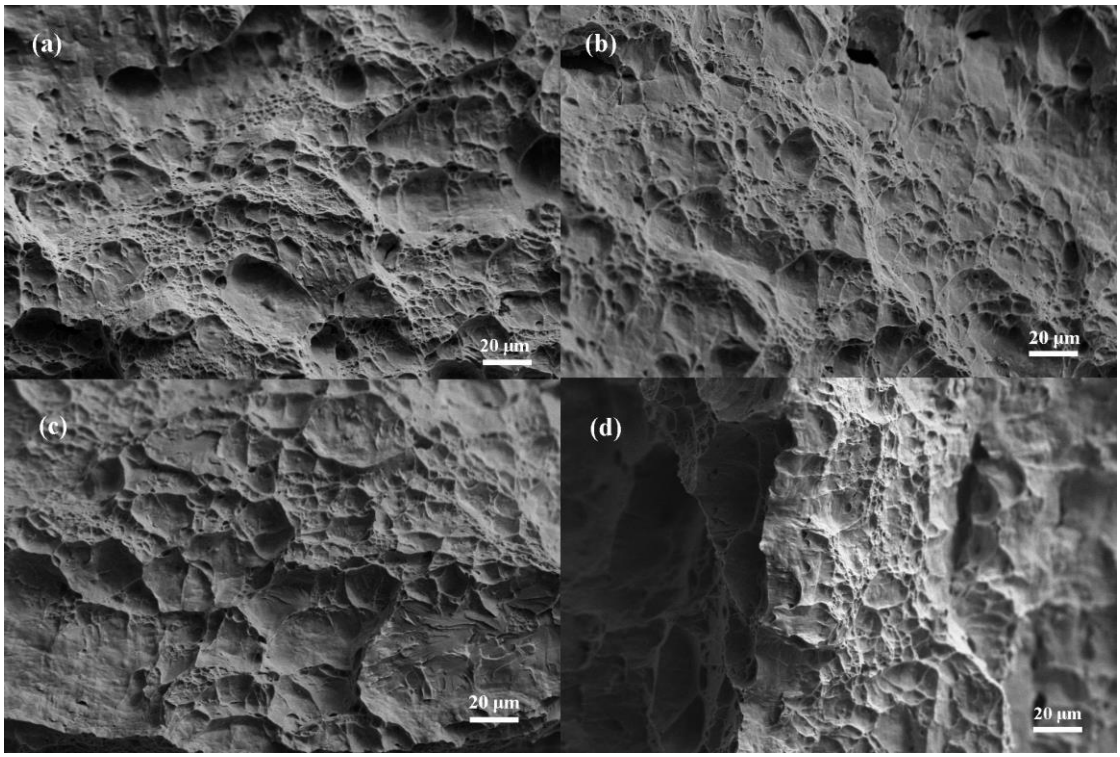

Figure 23. Microcosmic impact fracture morphology of X80 steel with different current densities (a) 0 mA/cm^2, (b) 2.53 mA/cm^2, (c) 4.60 mA/cm^2, (d) 6.03 mA/cm^2.

CHAPTER 5: CONCLUSIONS AND FUTURE WORK

5.1 Conclusions

1) X80 steel stretched in the air has typical tensile properties of ductile fracture with an ultimate tensile strength of 708±13.6% MPa, an elongation of 19.3±13.6% %, impact energy of 223±8.7% J at -10 ℃. Visible dimples were found at fracture surface. Steels suffered a significant loss of ultimate tensile strength, toughness and elongation in the hydrogen environment.

2) With a strain rate of 5 x 10^{-5} s^{-1}, the relative tensile strength and plasticity loss of X80 steel had no significant change within the range of assumed hydrogen partial pressures at room temperature, which can be explained as that the range of the assumed hydrogen partial pressure is relatively not large enough to be affected and the susceptibility of hydrogen embrittlement is more significant for steel has a UTS greater than 1000MPa. Dimples and cracks at fracture both were decreasing with the increasing hydrogen charging current density.

3) At room temperature, X80 steel had no apparent variation in ultimate tensile strength and elongation, except at the strain rate of 1 x 10^{-6} s^{-1}. The relative tensile strength and plasticity loss were enormous compared to the other test conditions, which was probably attributed to the rising time of charging hydrogen. Cracks and creep at fracture both were decreasing with the decreasing strain rate.

4) The fracture morphology of two test groups of X80 steel exhibited significant brittle rupture when tested with dynamic hydrogen charging.

5) The impact energy of X80 was not affected by hydrogen charging, which might due to the high deformation rate. Different current density also had no influence on the results of the impact test.

6) These observations suggest that hydrogen-charging time may be more critical for the X80 steel pipeline under the simulated service environment.

5.2 Future Work

More microstructure observation and discussion need to be done via light optical microscopy to determine if the microstructure of X80 steel has any difference after charging hydrogen. Learning the microstructure could also help engineer determining the embrittlement type and analyzing the mechanism of hydrogen embrittlement. Therefore, people could study out the prevention techniques for X80 steel under this circumstance.

Since this work concludes that the charging time may also affect the mechanical properties of X80 steel, there is a need to conduct research about the effect of hydrogen charging time on X80 steel under this condition. In this way, the service life of X80 steel for transporting SNG could be studied well.

Finally, evaluate the feasibility of applying the X80 steel to the new pipeline for transporting synthetic natural gas by analyzing the service environment of the new pipeline in China and the results from this thesis.

REFERENCES

[1] World Wide Web. West–East Gas Pipeline. Retrieved March 07, 2016, from https://en.wikipedia.org/wiki/West–East_Gas_Pipeline.

[2] Gray, H. R. (1974). Testing for hydrogen environment embrittlement: Experimental variables. In Hydrogen Embrittlement Testing. ASTM International.

[3] Nagpal, P., & Baker, I. (1991). The effect of strain rate on the room-temperature ductility of FeAl. Scripta metallurgica et materialia, 25(11), 2577-2580.

[4] Benson, R. B. (1968). Hydrogen embrittlement of stainless steel (High pressure hydrogen environment on tensile properties of stainless steel with and without strain induced martensite). AIME, TRANSACTIONS, 242, 2199-2205.

[5] World Wide Web. Hydrogen embrittlement. Retrieved March 07, 2016, from https://en.wikipedia.org/wiki/Hydrogen_embrittlement.

[6] Williams, D. P., & Nelson, H. G. (1970). Embrittlement of 4130 steel by low-pressure gaseous hydrogen. Metallurgical Transactions, 1(1), 63-68.

[7] Takasawa, K., Wada, Y., Ishigaki, R., & Kayano, R. (2010). Effects of grain size on hydrogen environment embrittlement of high strength low alloy steel in 45 MPa gaseous hydrogen. Materials transactions, 51(2), 347-353.

[8] Martin, M., Weber, S., Theisen, W., Michler, T., & Naumann, J. (2011). Effect of alloying elements on hydrogen environment embrittlement of AISI type 304 austenitic stainless steel. International Journal of Hydrogen Energy, 36(24), 15888-15898.

[9] Walter, R. J., & Chandler, W. T. (1971). Influence of hydrogen pressure and notch severity on hydrogen-environment embrittlement at ambient temperatures. Materials Science and Engineering, 8(2), 90-97.

[10] Atkinson, H. V., & Shi, G. (2003). Characterization of inclusions in clean steels: a review including the statistics of extremes methods. Progress in Materials Science, 48(5), 457-520.

[11] Kim, W. K., Koh, S. U., Yang, B. Y., & Kim, K. Y. (2008). Effect of environmental and metallurgical factors on hydrogen induced cracking of HSLA steels. Corrosion Science, 50(12), 3336-3342.

[12] Smialowski, M. (2014). Hydrogen in Steel. [Electronic Resource]: Effect of Hydrogen on Iron and Steel During Production, Fabrication, and Use. Burlington: Elsevier Science, 2014.

[13] World Wide Web. Mass diffusivity. Retrieved March 07, 2016, from https://en.wikipedia.org/wiki/Mass_diffusivity.

[14] Fick, A. (1855). Ueber diffusion. Annalen der Physik, 170(1), 59-86.

[15] Gorman, J. K., & Nardella, W. R. (1962). Hydrogen permeation through metals. Vacuum, 12(1), 19-24.

[16] Zheng, S., Zhou, C., Wang, P., Chen, C., & Chen, L. (2013) Effects of the Temperature on the Hydrogen Permeation Behaviours of L360NCS Pipeline Steel in 1MPa H2S Environments. International Journal Of Electrochemical Science, 8(2), 2880-2891.

[17] Heath, H. R. (1952). An experimental investigation of the diffusion of electrolytic hydrogen through metals. British Journal of Applied Physics, 3(1), 13.

[18] Smithells, C. J., & Ransley, C. E. (1935). The Diffusion of Gases through Metals. Proceedings of the Royal Society of London. Series A, Mathematical and Physical Sciences, (869), 172.

[19] Fowler, R. H., & Smithells, C. J. (1937). A Theoretical Formula for the Solubility of Hydrogen in Metals. Proceedings of the Royal Society of London. Series A, Mathematical and Physical Sciences, 37-47.

[20] Śmiałowski, M. (1962). Hydrogen in steel; effect of hydrogen on iron and steel during production, fabrication, and use. Oxford: Pergamon Press.

[21] Berry, B. S., & Pritchet, W. C. (1981). Effect of hydrogen on the magnetoelastic behavior of amorphous transitional metal-metalloid alloys.Journal of Applied Physics, 52(3), 1865-1867.

[22] Danford, M. D. (1992). The effect of tensile stress on hydrogen diffusion in metal alloys.

[23] Bockris, J. O., Beck, W., Genshawl, M. A., Subramanyan, P. K., & Williams, F. S. (1971). 19, 1209.

[24] Avery, M., Chui, B., Kariya, Y. G., & Larson, K. (2001). Hydrogen Induced Corrosion. Materials Science, 112.

[25] Sun, Y. W., Chen, J. Z., & Jun, L. I. U. (2015). Investigation into Hydrogen Diffusion and Susceptibility of Hydrogen Embrittlement of High Strength 0Cr16Ni5Mo Steel. Journal of Iron and Steel Research, International, 22(10), 961-968.

[26] Xuechong, R., Guangbin, S., Wuyang, C., Yanjing, S., Kewei, G., Lijie, Q., ... & Yinhui, C. (2005). Initiating, growing and cracking of hydrogen blisters. Chinese science bulletin, 50(17), 1962-1965.

[27] Ren, X. C., Chu, W. Y., & Su, Y. J. (2007). Effects of Atomic Hydrogen and Flaking on Mechanical Properties of Wheel Steel. Metallurgical & Materials Transactions. Part A, 38(5), 1004-1011.

[28] Chu, W. Y., Qiao, L. J., Chen, Q. Z., & Gao, K. W. (2000). Fracture and Environment Sensitive Fracture.

[29] Xiang, C. Y. (1999). Alloy Structural Steels. Metallurgical In-dustry Press, Beijing, 227.

[30] Louthan Jr, M. R. (2008). Hydrogen embrittlement of metals: a primer for the failure analyst. Journal of Failure Analysis and Prevention, 8(3), 289-307.

[31] Vasilenko, I. I., Karpenko, G. V., Mikitishin, S. I., & Tkachenko, N. N. (1966). Reversible and irreversible hydrogen embrittlement. Materials Science, 1(5), 430-431.

[32] Kolachev, B. A. (1979). Reversible hydrogen embrittlement of metals. Materials Science, 15(3), 202-207.

[33] ENG, S. B. (2014). HYDROGEN EMBRITTLEMENT IN STEEL FASTENERS.

[34] Ludwik, P. (1926), Embrittlement of steel by pickling. Z. Ver. Deutsch. Ing, 70, 379.

[35] Grant, N. J. and J. L. Lunsford (1955), Hydrogen embrittlement in cold-worked mild steel. Iron Age, 175, No 22, 92.

[36] Amiot, P. (1957), Fragility of α- structure steels owing to cold introduction of hydrogen. publs. Inst. Recherches siderurgie, Ser. A, No 158, pp 80.

[37] Skulev, P. V., L. I. Kvater and B. D. Peterov (1956), Effect of hydrogen on mechanical properties of steel. Problemy Metalloved. I Termichesk. Obrabotki, Sbornik, 141.

[38] Gao, H. (1995). Pipeline steel: Structure, property, and welding behavior. Shan Xi: Shanxi Science and Technology Publisher.

[39] Kumnick, A. J., & Johnson, H. H. (1975). Steady state hydrogen transport through zone refined irons. Metallurgical Transactions A, 6(5), 1087-1091.

[40] Zheng, S., Qi, Y., Chen, C., & Li, S. (2012). Effect of hydrogen and inclusions on the tensile properties and fracture behaviour of A350LF2 steels after exposure to wet H 2 S environments. Corrosion Science, 60, 59-68.

[41] Hardie, D., Charles, E. A., & Lopez, A. H. (2006). Hydrogen embrittlement of high strength pipeline steels. Corrosion Science, 48(12), 4378-4385.

[42] ASTM International. (2010). A370-10 Standard Test Methods and Definitions for Mechanical Testing of Steel Products. ASTM International.

[43] Wasserstein, R. L., & Lazar, N. A. (2016). The ASA's statement on p-values: context, process, and purpose. The American Statistician.

ABOUT THE AUTHOR

Xuan Li graduated from the Beijing Jiaotong University with a Bachelor Degree of Mechanical Engineering. During her undergraduate internship, she worked for Large Drive Business Unit, Siemens Ltd., China as a product manager assistant. After graduating from Beijing Jiaotong University, she is now studying in the University of South Florida pursuing master degree of Mechanical Engineering.